

Concentration-dependent short-range order in the relaxor ferroelectric (1-x)Pb(Sc, Ta)O₃-xPbTiO₃

Anatoly I. Frenkel,^{1,*} Douglas M. Pease,² Jayne Giniewicz,^{3,†} Edward A. Stern,⁴ Dale L. Brewe,^{4,5}
Million Daniel,² and Joseph Budnick²

¹*Department of Physics, Yeshiva University, New York, New York 10016, USA*

²*Department of Physics, University of Connecticut, Storrs, Connecticut 06269, USA*

³*Physics Department, Indiana University of Pennsylvania, Indiana, Pennsylvania 15705, USA*

⁴*Department of Physics, University of Washington, Seattle, Washington 98195, USA*

⁵*PNC-CAT, Argonne National Laboratory, Argonne, Illinois 60439, USA*

(Received 27 January 2004; revised manuscript received 29 March 2004; published 21 July 2004)

Using the x-ray diffraction and x-ray absorption fine structure techniques, we have probed Ti, Ta, and Sc local environments in the solid solution system (1-x)Pb(Sc, Ta)O₃-xPbTiO₃. This system is known to display a variety of ferroelectric behaviors ranging from variable order-disorder, to relaxor, to a mixed phase region, and then finally to normal ferroelectric, as the value of x is increased. We find, in agreement with neutron diffraction studies, no detectable displacements of Ta or Sc atoms from their oxygen cage centers in any of these systems. Surprisingly, we find that the Ti atom is displaced along (111) from its inversion symmetry center for $x=0.05$. However, this average local Ti displacement gradually changes from (111) to (001) as x increases, whereas the global crystal structure abruptly changes from rhombohedral to tetragonal at $x=0.45$. Our experimental results and theoretical modeling of others together suggest that this system consists of mixed regions, some characterized by a (111) Ti displacement and others characterized by a (001) Ti displacement. The displacement averaged over all regions becomes more weighted toward (001) as x increases. Another significant result is that all our samples (with x ranging from 0 to 0.5) have a high degree of local ordering of the B sites with alternate occupation of Ta and Sc atoms.

DOI: 10.1103/PhysRevB.70.014106

PACS number(s): 77.84.-s, 61.10.Ht, 78.70.Dm

INTRODUCTION

Relaxor ferroelectrics are a special class of ferroelectric materials, which typically have a perovskite or tungsten-bronze structure type, multiple ionic species on a particular crystallographic site, and distinctive material properties. Characteristic behavior is generally manifested in a diffuseness of the temperature dependence of the various properties that relate to the polarization of the material, and a strong frequency dependence of the dielectric response, particularly in the radio frequency range, as well as the persistence of a characteristic optical isotropy to temperatures well below that of the dielectric permittivity maximum.¹ These distinctive characteristics distinguish the relaxor ferroelectric from the so-called diffuse phase transition ferroelectric (DPTF) for which the diffuseness is related largely to macroscale inhomogeneity and other macroscale features. The origin of the characteristic behavior of the relaxor ferroelectric, on the other hand, lies in the interactions of polarized entities on a nanoscale. Materials exhibiting relaxor behavior are typically of a class of oxides referred to as “oxygen-octahedra compounds.”² The oxygen octahedron is simply a BO₆ unit where the six oxygen ions surround a particular transition metal ion, B (such as Ti, Ta, or Nb), so as to form an octahedral “cage.” All of the oxygen-octahedra structure-types are essentially composed of the basic oxygen-octahedral units linked in various configurations.

Two models that have been proposed to describe relaxor behavior are (1) the composition fluctuation model of Smolenskii *et al.*³ and (2) the polar region size effect model of

Cross.¹ In the composition fluctuation model, fluctuations in local composition lead directly to fluctuations in a local ferroelectric Curie temperature, and consequently to the observed gradual (relaxor), as opposed to sharp (classic ferroelectric), loss of spontaneous polarization as the temperature increases. In his polar region, size effect model, Cross has pointed out that for small scale polarized regions the energy barrier between different ion displacement directions becomes lowered, and such a region will not exhibit an averaged polar moment when this energy barrier is of the order $\sim kT$. This effect is an analog, for ferroelectricity, of the “blocking temperature” effect in ferromagnetism. In the magnetism case, the average ferromagnetic moment along a particular direction will become zero, at some critical temperature, for a small magnetic domain due to fluctuations in the moment direction. The critical temperature is smaller for smaller domain size. We point out that various probes such as neutron scattering⁴ and nuclear magnetic resonance⁵ indicate the existence of small polar regions in relaxors. These regions are lower-symmetry structural regions embedded in a surrounding higher symmetry matrix. The lower symmetry regions, when arranged in random orientations, will average to mimic higher symmetry structures such as cubic if observed using conventional x-ray diffraction (XRD).

We next contrast the properties of pure PbTiO₃ and pure Pb(Sc_{1/2}Ta_{1/2})O₃. Pure PbTiO₃ (PT) is a normal ferroelectric with a theoretical transition temperature of 763 K.⁶ In the ferroelectric tetragonal phase of PbTiO₃ the Ti atom is displaced relative to its oxygen cage along the cubic (001) direction. Recent studies by the x-ray absorption fine structure

(XAFS) technique have shown that locally both the Pb and Ti displacements in PbTiO_3 remain tetragonal and nonvanishing at temperatures above T_c , exhibiting distortions more than 70% of corresponding low temperature values, even though the XRD pattern is that of a cubic material.⁷ Pure $\text{Pb}(\text{Sc}_{1/2}\text{Ta}_{1/2})\text{O}_3$ (PST), on the other hand, can be forced into an ordered or disordered state, depending on annealing conditions.⁸ We now refer to PST in terms of the designation ABO_3 . If PST is disordered, the B site is randomly occupied by Ta and Sc and the material exhibits relaxor behavior. When ordered, on the other hand, PST shows superlattice lines and is a normal ferroelectric, for which the macroscopic easy axis of polarization is not (001), as in PT, but along the (111) body diagonal instead. Studies of single crystals find that, in the ferroelectric, ordered phase, PST shows a slight rhombohedral distortion from a perovskite structure,⁹ and ferroelectric PST is sometimes referred to as being in a “pseudocubic” structure.¹⁰ For disordered PST, which exhibits a relaxor behavior, Cross suggests a picture in which there are atomic displacements that dynamically change between different directions along the body diagonal of the perovskite cell.¹

Recent studies show that the nature of the relaxor behavior in PST is even more complex than modeled by Smolenskii or Cross. Dmowski *et al.* have shown by a combination of neutron and synchrotron based XRD that there is no detectable local displacement from the cube center for either Ta or Sc atoms, even for ordered material.¹¹ These authors do find a definite local displacement of the Pb atoms, but along (001), not the (111) direction which is the macroscopic direction of polarization. The authors state that “These results show that the conflict between the local structural preference and the average structure is not limited to relaxor ferroelectrics, but may be widely prevalent in mixed-ion ferroelectrics.” The XAFS results of Sicron *et al.* on pure PbTiO_3 show that with considerable accuracy, the “mixed ion” qualifier could be omitted from the above quotation.⁷

Given the above results, the unique characteristics of the $(1-x)\text{Pb}(\text{Sc}_{1/2}\text{Ta}_{1/2})\text{O}_3-x\text{PbTiO}_3$ solid solution, henceforth referred to as $(\text{PST})_{1-x}(\text{PT})_x$, make it an interesting system to study in that one traverses a variety of compositions that bridge the gap between the PST and PT materials. It has been observed that a variety of thermally “adjustable” states of structural ordering, Curie temperatures, and material properties are accessible for these materials. These properties make the system attractive for many device applications as well, and also as a useful model system for further exploring the fundamental nature of relaxor ferroelectrics.¹²

Initial studies on this system led to the identification of several distinct phase regions: There is a high-temperature cubic (nonferroelectric) phase. At room temperature there are several phases, depending on composition: (1) a rhombohedral (pseudocubic) region of variable order–disorder (VOD) involving the Sc and Ta ions at the B site of the perovskite structure ($x=0.0-0.075$), (2) a structurally invariable rhombohedral (pseudocubic) region ($x=0.1-0.4$), and (3) a tetragonal region extending from $x=0.45$ to $x=1$.¹² The three lower symmetry phase regions are separated by two boundary regions, the VOD boundary ($x=0.075-0.1$) and the mor-

photropic phase boundary (MPB) between $x=0.4$ and $x=0.45$.

A range of ferroelectric behaviors is observed for materials representing the three main noncubic phase regions of the system. Both relaxor and normal first order type responses occur for VOD compositions, with the as-fired (disordered) materials showing the diffuse, dispersive responses of a relaxor and the annealed (ordered) specimens exhibiting more sharp, first order type behaviors. Overall, as-fired (disordered) materials from the composition range $x=0.0-0.4$ display relaxor-type behavior, which becomes more normal on approaching the MPB ($x=0.4-0.45$), beyond which the response is essentially that of a first order ferroelectric. The variation of the ferroelectric response with heat treatment and/or composition is found to correlate with the coherence length of the ordering as determined by electron and x-ray diffraction.¹²

This study of the $(\text{PST})_{1-x}(\text{PT})_x$ system focuses on the local structure of the material as revealed by the x-ray absorption near edge structure (XANES) and extended x-ray absorption fine-structure (EXAFS) data and analysis carried out on selected ceramic specimens from each of the three phase regions of the system.

SAMPLE PREPARATION

The $(\text{PST})_{1-x}(\text{PT})_x$ ceramics ($x=0, 0.05, 0.1, 0.2, \text{ and } 0.5$) were prepared by a conventional mixed-oxide method involving the use of high-purity starting oxides (PbO , TiO_2 , Sc_2O_3 , and Ta_2O_5), a precursor phase formulation,¹³ and controlled lead atmosphere sintering. A wolframite (ScTaO_4) precursor was used in order to inhibit the formation of the undesirable, nonferroelectric pyrochlore phase. Each composition was calcined at 900°C for 4 hours and then at 1000°C for 1 hour with an intermediate comminution step. Compacted specimens of all compositions were then subjected to firing at 1400°C for 1 hour in sealed alumina crucibles containing $\text{Pb}(\text{Sc}_{1/2}\text{Ta}_{1/2})\text{O}_3\text{-PbZrO}_3$ source powders to control lead loss. Samples with compositions $x \geq 0.2$ were sufficiently dense ($\approx 95\%$ theoretical density) after this first sintering step, but specimens with compositions $x \leq 0.1$ required a second, higher temperature sintering ($1500^\circ\text{C}-1560^\circ\text{C}/20$ minutes), which was conducted in a molybdenum tube furnace with a relatively rapid heating and cooling schedule to avoid excessive lead loss. These samples had densities of 90–95% of the theoretical density following the second-stage sintering step. These samples were also subjected to a low temperature ($500^\circ\text{C}/20$ minutes) post-sintering anneal to relieve any stress that may have developed in the ceramic as a result of the rapid cooling at the conclusion of the second-stage sintering. Those specimens for which the degree of ordering could be varied by post-sintering heat treatment ($x < 0.1$) were annealed ($1000-1100^\circ\text{C}$) in a sealed system with a controlled lead atmosphere [$\text{Pb}(\text{Sc}_{1/2}\text{Ta}_{1/2})\text{O}_3\text{-PbZrO}_3$ source powders] so as to allow for negligible lead loss over the 10 hour period required to order the material. The ceramic specimens used in this study were in a range between ca. 0.5 to 3 mm thick and had areas ranging from 3 mm² to 100 mm².

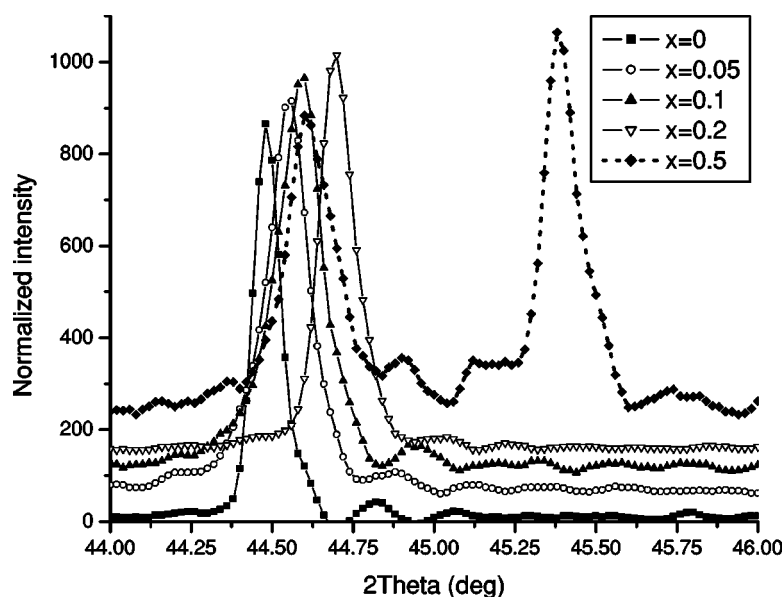


FIG. 1. XRD data obtained in $(\text{PST})_{1-x}(\text{PT})_x$ samples. Diffraction scans in the region of the (200) reflection, using a copper anode diffractometer with a curved graphite analyzer. The $K\alpha_2$ peak is stripped from the data, the plots are normalized to each other, and the data is given a minimal smoothing.

X-RAY DIFFRACTION MEASUREMENTS

X-ray diffraction studies were employed for all specimens to monitor for phase purity throughout the processing regimen, to determine structure type, lattice parameters, and x-ray densities, and to determine the degree of positional order of Sc and Ta for compositions in the VOD phase region. The initial x-ray characterizations were carried out when the samples were originally manufactured in the late 1980s.¹² These findings were well reproduced by our recent XRD studies. Complete solid solution was apparent for all compositions.

Pyrochlore is a common impurity phase in these materials. We have estimated the percentage pyrochlore phase by a standard method, which involves measuring the area under the perovskite (100) peak and comparing this area to the area of the nearby pyrochlore (222) peak.¹⁴ We stripped the $K\alpha_2$ lines from both peaks, and measured the areas relative to background. We used the method of estimation given by Yamashita,¹⁴

$$\text{Percentage pyrochlore} = 100 \left(1 - \frac{\text{Area}_{\text{perovskite}}}{\text{Area}_{\text{perovskite}} + \text{Area}_{\text{pyrochlore}}} \right). \quad (1)$$

Based on this method the percentage pyrochlore was 5% for PST with $x=0$, not detected for $x=0.05$, of order 1% or less for $x=0.1$, 7% for $x=0.2$, and not detected for $x=0.5$. In other words, the pyrochlore contamination is not systematic with Ti concentration, and does not exceed 7%. On the other hand, both the Ti K edge XAFS and the changes of the (200) XRD peak are quite systematic with Ti concentration, and we therefore conclude that the pyrochlore phase does not significantly influence our results.

Our XRD results are quite systematic in x . Ordered $\text{Pb}(\text{Sc}_{1/2}\text{Ta}_{1/2})\text{O}_3$ has a structure which consists of eight basic perovskite cells and, therefore, has a double supercell which can be indexed with accuracy using the cubic perovskite space group. The B-site cations alternate at the corners of the

simple cubic perovskite cells, and form alternate layers of Sc and Ta along the (111) directions of the supercell. The pure PST sample was slightly ordered, in that very weak superlattice peaks were observed, and no ordering between Sc and Ta sites was found for the other compositions. The structure observed by XRD was cubic for $x=0, 0.05, 0.1$, and 0.2 but becomes tetragonal for $x=0.5$ (Fig. 1). Our results confirm the previously measured lattice constants in this system which were determined with fine increment in x . In these measurements, it was shown that the transition from cubic to tetragonal phase is abrupt.¹²

Both our and previously measured diffraction scans in the region of the (200) reflection show a systematic shift of the peaks to higher angle as the lead titanate concentration increases. An important effect is a change from a cubic system to a tetragonal system for the $x=0.5$ concentration. We also observe, but do not interpret, subsplittings in the XRD of the tetragonal sample.

X-RAY ABSORPTION FINE-STRUCTURE MEASUREMENTS

Room temperature XAFS measurements of the three K edges (Ti, Ta, and Sc) were performed at Argonne National Laboratory's Advanced Photon Source (APS) and in Brookhaven National Laboratory's National Synchrotron Light Source (NSLS). The same samples were used for all measurements. Samples with $x=0.05, 0.1, 0.2$, and 0.5 were measured at the Ti K edge. Samples were measured at the Ta L_3 edge with $x=0, 0.05, 0.1, 0.2$, and 0.5 . Samples were measured at the Sc K -edge with $x=0, 0.05$, and 0.1 . As references, we used previously measured XAFS data of pure PbTiO_3 and EuTiO_3 .¹⁵

Ti K -edge measurements

Fluorescence Ti K -edge measurements of solid solutions of $(\text{PST})_{1-x}(\text{PT})_x$ samples were taken at the PNC-CAT's undulator beamline of the APS. The beam spot width at the

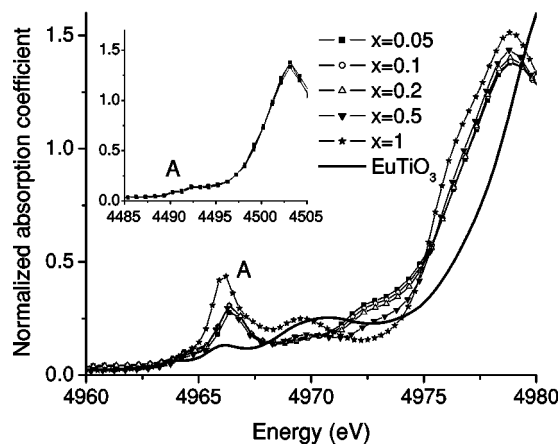
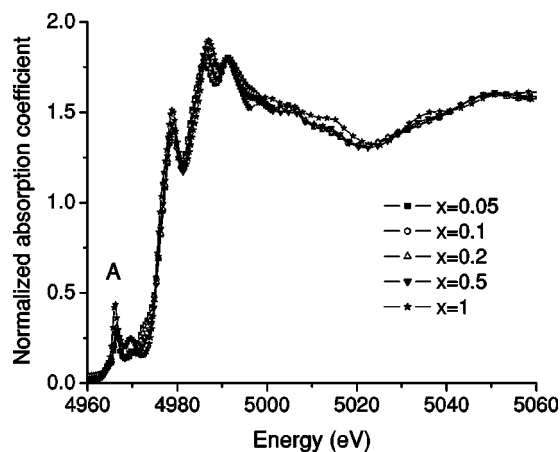


FIG. 2. Top, XANES spectra of Ti K edge in $(\text{PST})_{1-x}(\text{PT})_x$ samples. Feature A denotes the energy region of the dipole-forbidden, $1s-3d$ transition. Bottom: Blow-up region corresponding to the $1s-3d$ transition. Also shown is the reference Ti K -edge XANES in EuTiO_3 . The inset in the bottom pane shows the featureless $1s-3d$ transition region (A) in Sc K -edge XANES for $x=0, 0.05$, and 0.1 .

sample was about 0.6 mm horizontally and the beam intensity was 4×10^{13} photons/s. At relatively low PbTiO_3 concentrations of $x=0.05$ to 0.2 , an energy dispersive detector is required to separate Ti K_α fluorescence photons from the Sc K_α fluorescence photons that dominate the fluorescence background. We used a log-spiral of revolution (LSR) analyzer,¹⁶ designed and built for detection of Ti K_α photons. This device has now been markedly improved by the addition of a custom built annular ion chamber. The LSR performance was also improved by the addition of a feedback sample positioner that enabled reproducible and precise sample positioning. The optimum position of the sample was determined by maximizing the Ti signal relative to background. If the sample position was not optimized, pronounced Sc XAFS oscillations were observed at the Ti absorption edge, but these disappeared at optimum sample position. A beam stop was used to insure that only fluorescent x rays that first strike the LSR are detected; optimum positioning of the beam stop removed otherwise intense diffraction peaks. The LSR-ion chamber combination for Ti accepts about sixty percent of the available 2π solid angle,

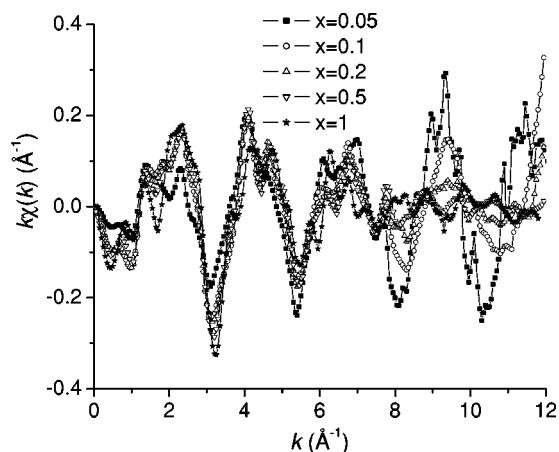


FIG. 3. Ti K -edge EXAFS: background subtracted and edge-step normalized $k\chi(k)$ in $(\text{PST})_{1-x}(\text{PT})_x$ samples.

and unlike standard energy dispersive detectors, does not saturate. The annular chamber was filled with a 80% Ar and 20% N_2 gas mixture. We know of no other detector setup that could successfully separate the dilute Ti XAFS signal from the otherwise overwhelming Sc signal. These studies showed no evidence of fluorescence distortion effects as expected because of the much larger absorption of the rest of the atoms compared to the Ti atoms. The XANES and EXAFS of all the spectra are shown in Figs. 2 and 3, respectively. The Fourier transform magnitudes of all the data are shown in Fig. 4.

Ta L_3 edge measurements

Ta L_3 edge of the same $(\text{PST})_{1-x}(\text{PT})_x$ samples (with $x=0, 0.05, 0.1, 0.2$, and 0.5) were measured at the bending magnet beamline X11-A of the NSLS. Fluorescence data were taken with an ionization chamber (Stern-Heald/Lytle detector) filled with Ar. A double-crystal Si(111) monochromator was used to tune the x-ray energy. The monochro-

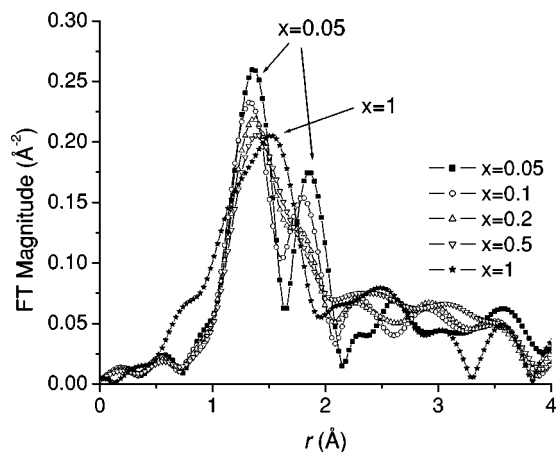


FIG. 4. Ti K -edge EXAFS: Fourier transform magnitudes of $k\chi(k)$ in $(\text{PST})_{1-x}(\text{PT})_x$ samples. Shown by arrows are groups of Ti–O distances that correspond to either (111) or (001) displacement of the Ti atom from the center of TiO_6 octahedron.

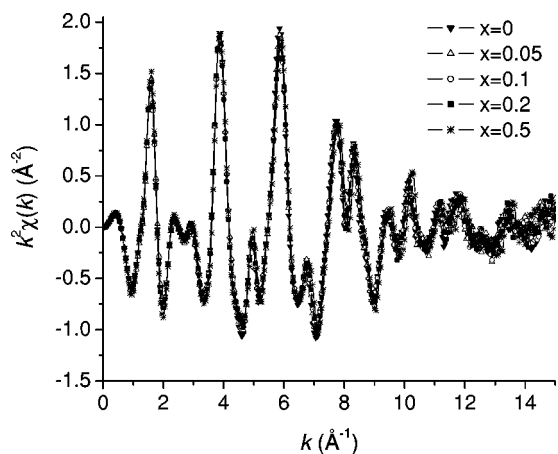


FIG. 5. Ta L_3 -edge EXAFS: background subtracted and edge-step normalized $k^2\chi(k)$ in $(\text{PST})_{1-x}(\text{PT})_x$ samples.

mator was detuned 25% to reject harmonics. In order to evaluate the effect of sample thickness on the absorption coefficient several successive scans were taken for different positions of the fluorescence detector including those where emergence angles of fluorescence rays were minimized. No diffraction peaks were detected. Comparison of the resultant absorption coefficients showed that the effect of the fluorescence geometry on the data was negligible. The EXAFS spectra and their Fourier transforms are shown in Figs. 5 and 6, respectively.

Sc K-edge measurements

Fluorescence Sc K -edge measurements of the $(\text{PST})_{1-x}(\text{PT})_x$ samples (at $x=0.05$ and 0.1) and pure PST ($x=0$) were taken at the PNC-CAT's bending magnet beamline at the APS, using a single-channel Ge detector. The samples were spun to remove Bragg peaks. Up to 50 measurements were averaged to obtain the absorption coefficient data at each concentration. At $x=0.05$ and 0.1 , the data

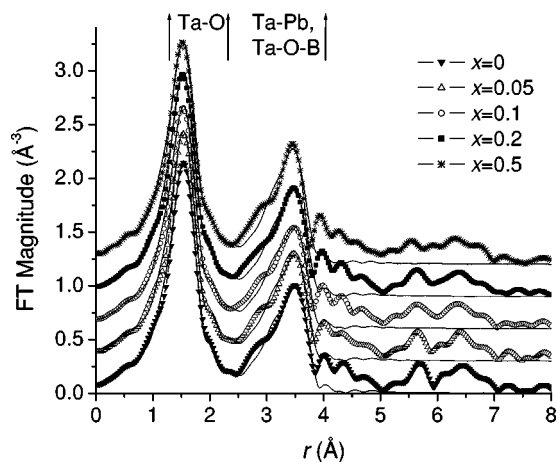


FIG. 6. Ta L_3 -edge EXAFS: Fourier transform magnitudes of $k^2\chi(k)$ in $(\text{PST})_{1-x}(\text{PT})_x$ data (symbols) and FEFF theory (solid). The two r -ranges, marked by arrows, correspond to the two stages of the fitting procedure as described in the text.

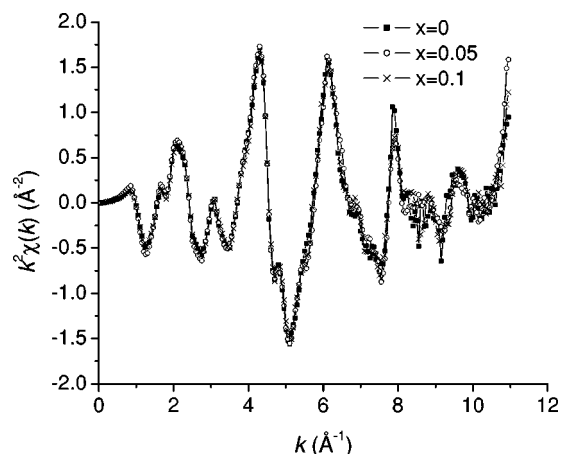


FIG. 7. Sc K -edge EXAFS: background subtracted and edge-step normalized $k^2\chi(k)$ in $(\text{PST})_{1-x}(\text{PT})_x$ samples.

ranges were limited by the occurrence of Ti K -edge (4966 eV) that corresponds to the data truncation at k_{max} of ca. 11\AA^{-1} during the data analysis. To evaluate the effect of self-absorption distortion, some measurements were also performed with the ionization chamber in a different geometry. Comparison of the measured absorption coefficients showed that the effect of the fluorescence geometry and fluorescent detector on the data were negligible, thus assuring that any distortion effects were negligible. The XANES spectra are shown in the inset of Fig. 2. The EXAFS spectra and their Fourier transforms are shown in Figs. 7 and 8, respectively.

DATA ANALYSIS

Ti K-edge and Sc K-edge XANES

Ti K -edge XANES data of all the samples, from $x=0.05$ to 1 (Fig. 2), have a feature "A" located in the region corresponding to the $1s-3d$ transition. This transition is dipole forbidden in the atom by the $\Delta L=1$ selection rule. In order to

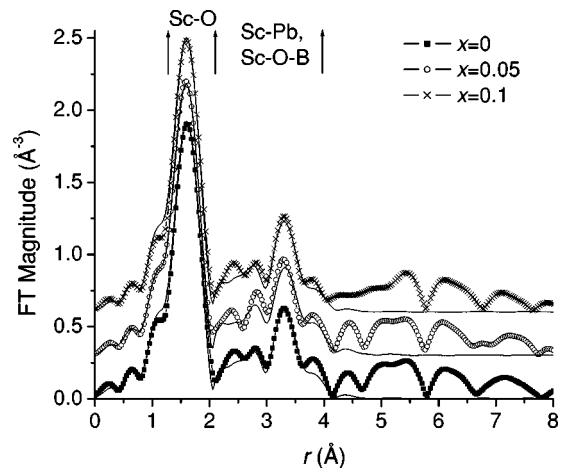


FIG. 8. Sc K -edge EXAFS: Fourier transform magnitudes of $k^2\chi(k)$ in $(\text{PST})_{1-x}(\text{PT})_x$ data (symbols) and FEFF theory (solid). The two r ranges, marked by arrows, correspond to the two stages of the fitting procedure as described in the text.

TABLE I. Ti atom displacements in $(\text{PST})_{1-x}(\text{PT})_x$ calculated using Eq. (3).

x	0.05	0.1	0.2	0.5	1
$d, \text{\AA}$	0.22(2)	0.24(2)	0.24(3)	0.23(2)	0.31(3)

contribute significantly to XANES in this region, p character of the final state of the photoelectron has to be added in the solid. The solid can add p character in this region due to hybridization between Ti $3d$ and O $2p$ orbitals¹⁷ if the Ti atom is displaced away from the inversion symmetry center of the TiO_6 octahedra. The presence of a large peak in the energy range “A” is, therefore, a signature of displacement of the Ti atoms from an inversion symmetric site. As pointed out,¹⁸ even a centrosymmetric perovskite such as EuTiO_3 has a small peak in the same energy region due to vibrational disorder within the TiO_6 octahedron. References 18 and 19 find that for polycrystalline perovskites, the off-center displacement d_i (static and/or dynamic) of the Ti atom from the center of the TiO_6 octahedron is related to the area A_i under the corresponding peak in the $1s-3d$ transition region,

$$A_i = \frac{\gamma_i}{3} d_i^2, \quad (2)$$

where i denotes a specific perovskite system (we use $i = “E”$ for EuTiO_3 and “P” for PbTiO_3) and γ_i is a proportionality constant measured for different perovskites.¹⁸ $\gamma_E = 13.6 \pm 2.8 \text{ eV/\AA}^2$ and $\gamma_P = 12.3 \pm 1.4 \text{ eV/\AA}^2$.

The area under the peak “A” can be used to characterize the displacement of the resonant atom from the inversion symmetry center. It never completely vanishes, even for perovskites with no static displacements, because of thermal vibrations of Ti with respect to the octahedral cage. In the Ti K -edge XANES data of all the samples, from $x=0.05$ to 1 (Fig. 2), the intensity of the signal in this region is much larger than in the reference, cubic EuTiO_3 system. Since all the samples were measured at the same temperature, the cause of the difference is the different magnitude of static Ti displacement off the TiO_6 octahedron center. Using Eq. (2) and the experimentally determined value for the reference (dynamic) Ti atom displacement $d_E = 0.103 \text{ \AA}$ in EuTiO_3 at room temperature,¹⁸ we can obtain the Ti displacements d_P for all x in the $(\text{PST})_{1-x}(\text{PT})_x$ system through the difference between the areas of feature A in Fig. 2 for $(\text{PST})_{1-x}(\text{PT})_x$ data and EuTiO_3 data,

$$\Delta A = \frac{\gamma_P}{3} d_P^2 - \frac{\gamma_E}{3} d_E^2. \quad (3)$$

Using Eq. (3) and Ti XANES data of $(\text{PST})_{1-x}(\text{PT})_x$ system (Fig. 2) we obtained the Ti atom displacements (Table I). As a cross-check of the validity of these results obtained by XANES analysis, the displacement obtained for Ti in pure PbTiO_3 is in excellent agreement with crystallographic data (0.308 \AA).²⁰ This agreement shows that the above procedure is a reliable method to determine the Ti displacement magnitude. As discussed below, for polycrystalline and cubic materials this method is not sensitive to the direction of Ti atom

displacement, but if complemented by EXAFS analysis of the same system, both techniques can quantify both the direction and the magnitude of the Ti atom displacement.

The bottom pane of Fig. 2 shows both Ti K -edge and Sc K -edge XANES spectra. The magnitude of the pre-edge feature A is markedly lower in the Sc XANES signal compared to its counterpart in the Ti K -edge XANES. Since Sc and Ti are neighbors in the periodic table and their nearest neighbors in the $(\text{PST})_{1-x}(\text{PT})_x$ system are the same (oxygen and lead), one would expect that the mixing of O $2p$ states with Sc $3d$ states will be of the same magnitude as for Ti. Based on that and on the previous discussion of the relation between the area of the pre-edge feature and the magnitude of the B-ion off-center displacement [Eq. (2)], this Sc K -edge XANES data is consistent with much smaller, if any, off-center displacements of Sc atoms, compared to Ti atoms.

Ti K -edge EXAFS first shell analysis

For each measured x-ray absorption spectrum, the AUTOBK code²¹ was used to normalize the absorption coefficient, $\mu(k)$, and separate the EXAFS, $\chi(k)$, from the isolated atom absorption background, $\mu_0(k)$. This process is shown in the following relation:

$$\chi(k) = \frac{\mu(k) - \mu_0(k)}{\Delta\mu_0(k)}, \quad (4)$$

where k is the photoelectron wave number, $k = \sqrt{2m(E - E_0)/\hbar^2}$, E is the photon energy, and E_0 is the photoelectron energy origin (chosen at the middle of the absorption edge jump). The background function, $\mu_0(k)$, was obtained by minimizing the signal in the low- r region of the Fourier-transformed $\chi(k)$ data. $\Delta\mu_0(k)$ is the absorption edge step (K edge for Ti and Sc, and L_3 edge for Ta).

The EXAFS signal, $\chi(k)$, which is the sum of all contributions, $\chi_i(k)$, from groups of atoms that lie at approximately equal distances from the absorbing atom (i.e., the i th shell) was adjusted by applying the EXAFS equation, written in the following extended form:

$$\chi(k) = \sum_i \frac{S_0^2 N_i}{k R_i^2} |f_i^{\text{eff}}(k)| \sin[2kR_i + \delta_i(k)] e^{-2\sigma_i^2 k^2} e^{-2R/\lambda_i(k)}, \quad (5)$$

where k is the photoelectron wave number, $f_i^{\text{eff}}(k)$ and $\delta_i(k)$ are the photoelectron scattering-path amplitude and phase, respectively, S_0^2 is the passive electron reduction factor, R_i is the effective half-path-length (which is equal to the interatomic distance for single-scattering paths), σ_i^2 is the mean-square deviation in R_i , and $\lambda_i(k)$ is the photoelectron mean free path. Theoretical amplitudes $f_i^{\text{eff}}(k)$, and phases $\delta_i(k)$, for the absorbing atom in a specific model structure had been calculated with FEFF6²² and the so constructed theoretical EXAFS signal [Eq. (5)] was used to fit the experimental $\chi(k)$ data using the FEFFIT program.

Before the quantitative analysis, a few important observations had been made based on the visual examination of both the XANES and EXAFS Ti K -edge data. Namely, one can

TABLE II. The values used in the Fourier transforms and the FEFFIT fits for the Ti K -edge EXAFS data (at $x=0.05$): k range (Δk) and k -weighting (k^w), the fitting range (ΔR), the number of independent data points (N_{idp}), the number of fitting parameters (P), the reduced chi-squared (χ_v^2) and R factor (R). For $x=0.1, 0.2, 0.5$, and 1.0 the Fourier transforms (Fig. 4) were performed with the same parameters as for the $x=0.05$.

X	Δk (\AA^{-1})	k^w	ΔR (\AA)	N_{idp}	P	χ_v^2	R
0.05	3–10	k	1–2.4	8	4	218	0.07

suggest that the $x=0.05$ spectra are consistent with Ti displaced in the (111) cubic direction, while at relatively large concentrations, $x=0.2$ and 0.5, the direction of Ti atom displacement is approaching the (001) cubic direction. Indeed, the EXAFS data (Figs. 3 and 4) demonstrate that when the concentration increases from $x=0.2$ to 0.5, the Ti environment becomes very similar to that in pure tetragonal PbTiO_3 that has Ti displaced in (001) direction from the center. At low concentrations, the data look quite different from that in pure PbTiO_3 , namely, the split of the first Ti–O coordination shell in two groups of distances is apparent. The data at $x=0.05$ can be qualitatively explained if we recall that the displacement of Ti along the (111) cubic direction would result in splitting the sixfold degenerate (in the cubic structure) Ti–O distances in two groups: three short Ti–O1 distances and three long Ti–O2 distances. When the distortion is in the (001) direction, Ti is getting closer to one axial oxygen, farther away from another axial oxygen, and the third group of distances is that between Ti and four equatorial oxygens, therefore the splitting is in three groups: one Ti–O1, four Ti–O2, and one Ti–O3. In EXAFS, excellent spatial resolution is required to observe such splitting, especially because the most degenerate (fourfold) group will dominate the radial distribution. Therefore, not being able to observe a visible splitting in $x=0.2$, $x=0.5$, and $x=1$ data is consistent with either tetragonal or cubic (where the splitting does not exist) structure. However, by the examination of Ti K -edge XANES data we concluded above that the Ti atoms

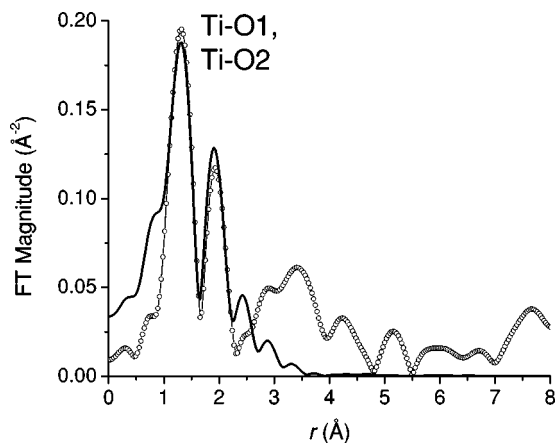


FIG. 9. Ti K -edge EXAFS analysis: Fourier transform magnitudes of the $k\chi(k)$ data (symbols) and FEFF theory (solid) for $x=0.05$ in a $(\text{PST})_{1-x}(\text{PT})_x$ sample.

TABLE III. The values used in the Fourier transforms and the FEFFIT fits for the first nearest neighbor Ta L_3 -edge EXAFS data analysis: k range (Δk) and k weighting (k^w), the fitting range (ΔR), the number of independent data points (N_{idp}) per data set, the number of fitting parameters (P) per data set, the total reduced chi-squared (χ_v^2), and R factor (R) per data set. Since the fits were performed concurrently for all five data sets, P is a fractional number.

X	Δk (\AA^{-1})	k^w	ΔR (\AA)	N_{idp}	P	χ_v^2	R
0	2.5–13	k^2	1.3–2.3	8.15	2.4	26	0.0026
0.05	2.5–13	k^2	1.3–2.3	8.15	2.4	26	0.0019
0.1	2.5–13	k^2	1.3–2.3	8.15	2.4	26	0.0016
0.2	2.5–13	k^2	1.3–2.3	8.15	2.4	26	0.0030
0.5	2.5–13	k^2	1.3–2.3	8.15	2.4	26	0.0028

are displaced from the cubic center at all concentrations. Moreover, since PbTiO_3 is known to be tetragonally distorted at room temperature, with the Ti atom displaced in the (001) direction, it is, therefore, logical to expect a similar displacement of the Ti atom in both $x=0.2$ and 0.5 data that progressively resemble PbTiO_3 data as x increases. To speculate further, we may suggest that the crossover region, when the orientation of the Ti displacement changed from (111) to (001) is between $x=0.1$ and $x=0.2$ because the $x=0.1$ data very much resemble the smallest concentration, $x=0.05$ since both data sets display distinct splitting of the first shell peak into two peaks.

Theoretical scattering amplitudes of Ti–O nearest neighboring shell were calculated with FEFF6 in the approximation that Ti occupies the B site of ABO_3 in the perovskite unit cell of $\text{Pb}(\text{Sc}, \text{Ta})\text{O}_3$ with $a=4.07$ \AA . The model of Ti environment was constrained by allowing the Ti displacement to be in the (111) cubic direction only. Fits of the FEFF6 theory to the data were performed in r space. The parameters of the Fourier transform (the data ranges in k and r spaces, the number of relevant independent points in the data, the number of fitting parameters, as well as the reduced chi-squared and the R factor are reported in Table II. Although the R factor (0.07) is quite large (the data were much noisier than at other atoms' absorption edges due to the much lower concentration of Ti), and there is a large uncertainty in the amplitude of EXAFS signal, there is not a large uncertainty in the distances. The separation between the two Ti–O subshells, Ti–O1 and Ti–O2, is defined by EXAFS with even smaller error than the error in the Ti–O1 and Ti–O2 distances themselves.

We varied the two groups of Ti–O distances that correspond to the two groups of three oxygen atoms in each that form faces of TiO_6 octahedron that are perpendicular to the (111) direction of Ti displacement. If the magnitude d of Ti displacement from the center of the octahedron were zero, the two distances, Ti–O1 and Ti–O2, would be the same: 2.035 \AA . However, from the analysis of the $x=0.05$ data (Fig. 9) we obtained the result that these distances are 1.91(3) \AA and 2.17(4) \AA with the splitting δ equal 0.26(4) \AA . These results would be in excellent agreement with our Ti XANES data analysis [$d=0.22(2)$ \AA] if one as-

TABLE IV. Structural results obtained by Ta L_3 -edge EXAFS data analysis. The Ta–O first nearest neighbor distance (marked by arrows in Fig. 6) and its disorder were obtained by the concurrent, five-data-set analysis. The Ta–Pb and Ta–Sc distances were obtained separately, as described in the text below. The last column has the values of the pseudocubic lattice constants a , obtained by XRD (Ref. 23).

x	Ta–O		Ta–Pb		Ta–Sc, Ta–O–Sc		$a, \text{\AA}$
	$r, \text{\AA}$	$\sigma^2, \text{\AA}^2$	$r, \text{\AA}$	$\sigma^2, \text{\AA}^2$	$r, \text{\AA}$	$\sigma^2, \text{\AA}^2$	
0	1.961(2)	0.0064(3)	3.59(1)	0.0112(20)	4.032(5)	0.0087(7)	4.074
0.05	1.959(3)	0.0066(4)	3.59(1)	0.0119(22)	4.028(5)	0.0089(8)	4.063
0.1	1.958(3)	0.0071(4)	3.59(2)	0.0121(26)	4.028(6)	0.0092(9)	4.060
0.2	1.957(2)	0.0071(4)	3.60(2)	0.0125(31)	4.026(6)	0.0087(10)	4.051
0.5	1.954(3)	0.0071(4)	3.59(2)	0.0123(38)	4.010(7)	0.0082(11)	

sumes the (111) direction of Ti atom displacement.

We would like to emphasize the difference between the bond length split δ of the two Ti–O subshells and the magnitude d of the Ti atom displacement. The quantity δ is measured along the cubic (001) directions, and d along the (111) direction, so they are related to each other as follows: $\delta = 2d/\sqrt{3}$. Using the experimentally determined value of $d = 0.22(2)$ Å, the magnitude of $\delta = 0.25(2)$ Å predicted by this relation is in excellent agreement with the EXAFS analysis result [0.26(4) Å] obtained assuming the (111) Ti displacement. Indeed, the short and long Ti–O distances calculated assuming the (111) direction of Ti displacement by $d = 0.22$ Å are 1.90 Å and 2.15 Å, respectively, i.e., very close to those experimentally obtained by EXAFS analysis. This agreement also independently shows that Ti is displaced in the (111) direction.

Ta L_3 -edge EXAFS first shell analysis

Since the raw Ta L_3 -edge EXAFS data do not indicate any visible splitting of the Ta–O shell (Fig. 6), in contrast to the Ti EXAFS data (Fig. 4), the Ta first shell analysis was performed by assuming a single, sixfold degenerate Ta–O bond in FEFF6 modeling. To lower the uncertainties and to improve confidence in the best-fit results, we analyzed all the five data sets concurrently, by applying physically reasonable constraints (e.g., that the energy origins E_0 and the passive electrons amplitude reduction factors S_0^2 are the same in all five data sets) in the fit process. The characteristics of Fourier transforms and fitting procedure are summarized in Table III.

As a result of fitting theory to data (Fig. 6), we obtained that the Ta–O distance is gradually decreasing (as a function of Ti concentration) from 1.961(2) Å at $x=0$ to 1.954(3) Å at $x=0.5$ (Table IV).]

Sc K -edge EXAFS first shell analysis

As suggested by visual absence of any splitting of the Sc–O shell (Fig. 8), the first shell analysis of Sc K -edge EXAFS data of the samples with $x=0$, 0.05, and 0.1 was performed by assuming a single, sixfold degenerate Sc–O bond in FEFF6 calculations, similar to the Ta L_3 -edge EXAFS analysis. This model is very reasonable because it is

also consistent with Sc K -edge XANES data that showed no pre-edge feature that would indicate a significant off-center displacement of Sc atom. We have minimized the uncertainties in the best-fit values of fitting parameters by concurrently analyzing all three data sets, similar to the procedure used in Ta L_3 -edge EXAFS data analysis. Analogously, the E_0 and S_0^2 were constrained to be the same for all the three sets. The characteristics of Fourier transforms and fitting procedure are summarized in Table V.

From our analysis we deduce that the Sc–O distance is almost constant as a function of Ti concentration and is equal to 2.104(4) Å for pure PST (Table VI). The smaller than expected best-fit values of the σ^2 reveal the correlation of this parameter with another amplitude factor, S_0^2 [that was obtained to be 0.61(2) in the result of the three data sets fit]. Since both factors do not affect the phase of the EXAFS oscillations [Eq. (5)], the accuracy in the determination of the Sc–O bond lengths was unaffected.

DISCUSSION

Dmowski *et al.* do not observe a (111) displacement for Ta or Sc sites in pure PST in their neutron diffraction results.¹¹ This finding is in agreement with our XAFS results. Dmowski *et al.* do observe a local Pb displacement; however the Pb displacement is along (001) despite the fact that the overall crystalline distortion is along (111). Evidence for local Pb shifts was also obtained by the pair distribution func-

TABLE V. The values used in the Fourier transforms and the FEFFIT fits for the first nearest neighbor Sc K -edge EXAFS data analysis: k range (Δk) and k weighting (k^w), the fitting range (ΔR), the number of independent data points (N_{idp}) per data set, the number of fitting parameters (P) per data set, the total reduced chi-squared (χ_v^2), and R factor (R) per data set. Since the fits were performed concurrently for all three data sets, P is a fractional number.

x	$\Delta k (\text{\AA}^{-1})$	k^w	$\Delta R (\text{\AA})$	N_{idp}	P	χ_v^2	R
0	2–10	k^2	1.3–2.0	5.13	2.67	25	0.0024
0.05	2–10	k^2	1.3–2.0	5.13	2.67	25	0.0013
0.1	2–10	k^2	1.3–2.0	5.13	2.67	25	0.0019

TABLE VI. Structural results obtained by Sc K -edge EXAFS data analysis. The Sc–O first nearest neighbor distance (marked by arrows in Fig. 8) and its disorder were obtained by the concurrent, three-data-set analysis. The Sc–Pb and Sc–Ta distances were obtained separately, as described in the text below. The last column has the values of the pseudocubic lattice constants a , obtained by XRD (Ref. 23).

x	Sc–O		Sc–Pb		Sc–Ta, Sc–O–Ta		$a, \text{\AA}$
	$r, \text{\AA}$	$\sigma^2, \text{\AA}^2$	$r, \text{\AA}$	$\sigma^2, \text{\AA}^2$	$r, \text{\AA}$	$\sigma^2, \text{\AA}^2$	
0	2.104(4)	0.0001(7)	3.37(2)	0.085(21)	4.06(4)	0.0142(51)	4.074
0.05	2.095(3)	0.0005(5)	3.38(3)	0.0095(27)	4.05(3)	0.0113(42)	4.063
0.1	2.099(3)	0.0003(5)	3.37(2)	0.0085(20)	4.07(4)	0.0142(50)	4.060

tion analysis by Teslic *et al.*,²⁴ in the analogous system, $\text{PbZr}_{1-x}\text{Ti}_x\text{O}_3$ or PZT. We also note that in pure PbTiO_3 , Sicron *et al.* observed a local Ti displacement along (001) for all temperatures, even temperatures above T_C .⁷ With these studies in mind we note that in our PST-PT system, we find for the first time a local (111) displacement of an ion in this perovskite ferroelectric system; that is to say we observe that the Ti ion displaces along (111) for the lowest Ti concentration. The combination of EXAFS and XANES shows that the Ti ion remains off center for all x . The average Ti displacement systematically changes from (111) to (001) as x increases, despite the fact that the crystal structure abruptly changes to tetragonal when one goes from $x=0.2$ to $x=0.5$.¹² A model of relaxor ferroelectrics due to Cross¹ suggests that small polar regions may dynamically change their direction of ionic displacement between different orientations. In pure PST these different directions would be along the different (111) body diagonals. In this picture, there is a potential barrier between different displacement directions, and this barrier can be of the order $\sim kT$ if the polar region is sufficiently small. Maaskant and Bersuker²⁵ have formulated an exactly solvable theory of an ion in an isolated regular oxygen octahedron. In their model, one could have energy minima both for tetragonal (001) and trigonal (111) displacements, but no intermediate solutions.

We would like to acknowledge recent x-ray and neutron diffraction studies of other solid solutions with MPBs [e.g., PZT, $(1-x)\text{Pb}(\text{Mg}_{1/3}\text{Nb}_{2/3})\text{O}_3$ - $x\text{PbTiO}_3$, or PMN-PT, and $(1-x)\text{Pb}(\text{Zn}_{1/3}\text{Nb}_{2/3})\text{O}_3$ - $x\text{PbTiO}_3$, or PZN-PT] have reported monoclinic phase in the vicinity of their MPBs below room temperature.²⁶ Theoretical calculations reproduce this new monoclinic phase,^{27–32} and obtain that it mediates rotation, on the atomic scale, of the B atoms from (111) to (001) directions.^{27–30} We found no direct evidence from our EXAFS data that such rotation is possible in PST-PT (because of the inadequate spatial resolution of Ti K -edge EXAFS for such a determination). However, we do find that the changes in the radial distribution of Ti (Fig. 4), when x increases, can be fit by a superposition of the spectra from the $x=0.05$ and $x=1$ samples with weights varying with x , consistent with the Maaskant-Bersuker model. Indeed, in the framework of this model, a gradual change, observed by EXAFS, in average Ti displacement from (111) to (001) as x increases may be explained by the co-existence of small regions of (001) and (111) displacements in the same material. The average would become more weighted toward the (001)

displacement as x increases. That implies that the rhombohedrally distorted, quasicubic PtTiO_3 perovskite units will be present in the samples at concentrations x up to 0.5 and higher. It is possible that the occurrence of the peaks (shown by arrows in Fig. 4) in Fourier transformed EXAFS at all concentrations up to 0.5 is the manifestation of these local (111) displacements and, therefore, the validity of Maaskant-Bersuker model.

One question that arises is how one models the fact that, for small Ti concentrations, the energetics favor a (111) Ti displacement and for large Ti concentration a (001) displacement. We suggest an analogy with the alloy system in which Fe precipitates are developed in a Cu matrix. Although bulk room temperature Fe is bcc, the energies of bcc and fcc Fe are close enough that the interfacial energies drive the Fe to the fcc structure if there is a small Fe cluster embedded in a Cu matrix.³³ In the present case, we suggest that nanoscale PbTiO_3 regions when forced to expand so as to interface with the surrounding PST matrix would take on the (111) distorted, rather than the (001) distorted structure.

Another interesting observation is that the Ta–O distance (1.96 Å) is smaller than half the lattice parameter of pure PST. In a cubic (or in a quasicubic) ABO_3 perovskite with the lattice parameter of ca. 4.07 Å, the B–O distance should be 2.035 Å. In our case, the Ta–O distance is 0.075 Å shorter than half the lattice parameter. Our hypothesis (that will be corroborated by the Sc K -edge EXAFS analysis as described below) is that this finding indicates the high degree of ordering on the B site in the pure PST. Indeed, if Sc and Ta atoms are ordered and alternately occupy neighboring B sites, then the majority of B–O–B' linkages in a (001) cubic direction are Sc–O–Ta linkages. In such an ordered model, the B–O–B' linkages in their quasi cubic environment are approximately collinear and the B–O–B' distance should be equal to the lattice parameter of the average lattice, i.e., the Sc–O–Ta length should be about 4.07 Å, leading to a Sc–O distance of 2.11 Å. This prediction from the B-site ordering model is in excellent agreement with our EXAFS-determined Sc–O distance of 2.104(4) Å. In other words, if we add our Ta–O distance determined from XAFS to our Sc–O distance, the sum equals the lattice parameter to within our error bars. This result indicates that we do not have many contributions from disordered Sc–O–Sc or Ta–O–Ta linkages. Moreover, the difference of 0.14 Å in the so obtained Sc–O and Ta–O bond lengths is consistent with the difference of 0.105 Å in Sc^{3+} and Ta^{5+} ionic radii values (0.745 Å and

0.64 Å,³⁴ respectively). Thus, the shortening of the experimentally obtained Ta–O distance relative to the average B–O distance in the ABO₃ perovskite is compensated by elongating the Sc–O bonds, consistent with the Ta and Sc size mismatch. This in turn, is evidence that the local structure of pure PST is highly ordered. A similar effect (shortening of Nb–O bond from the nominal half-lattice parameter value) in another relaxor system, lead-magnesium niobate Pb(Mg_{1/3}Nb_{2/3})O₃, or PMN, was previously observed by diffraction anomalous fine structure measurements.³⁵ In that case, Nb and Mg ion radii are in a similar relation to our Ta and Sc, respectively. This, and another similar mixed perovskite system [Pb(Mg_{1/2}W_{1/2})O₃-Pb(Ni_{1/3}Nb_{2/3})O₃-PbTiO₃ called PMW-PNN-PT] are known to have locally B-site ordered nanodomains.³⁶ Because XAFS is a local probe (within ca. 5 Å around the central atom) the comparison of XAFS and XRD results is strong evidence that our pure PST sample also consists of locally B-site ordered regions of correlation lengths of at least several lattice constant distances, i.e., nanoscale lengths.

The combined length of the B–O and B'–O bonds is thus a reliable measure of relative degree of ordering in the PST and analogous mixed B-site perovskites. If their sum is greater than the lattice parameter, the B–O–B' linkage will not be collinear and it will thus indicate that a significant amount of structural disorder is present. Dmowski *et al.* studied the structure of their partially ordered PST sample and reported it to be locally distorted.¹¹ In their work, they observed that both Sc–O and Ta–O bonds are longer than the average B–O distance and concluded that BO₆ octahedra rotate and thus form noncollinear B–O–B' linkages.

Note that in Fig. 4 the Ti *K*-edge EXAFS shows dramatic changes in the region up to $r \sim 2.2$ Å as a function of x while from Figs. 6 and 8 much smaller changes as a function of x occur up to $r \sim 4$ Å indicating that little changes are occurring around both the Ta and Sc atoms, respectively. In the latter cases the region with little change includes the B–O–B' bonds, suggesting that the order occurring in the pure PST persists to a significant degree in other (PST)_{1-x}(PT)_x samples even up to $x=0.5$. To confirm this possibility the analysis about the Ta and Sc atoms was extended to cover the B–O–B' bonds to $r=4.0$ Å (Figs. 6 and 8, respectively). FEFF6 calculations were performed by replacing B atoms in the third nearest neighbor (3NN) position to the central (absorbing) B atom in the cubic perovskite structure of PbBO₃ by B'. The most important interactions in the distance range from the 1NN through the 3NN shell were found to be B–Pb(2NN) and B–B' (3NN). The latter contribution to EXAFS has the same half-path length as the collinear double-scattering and triple-scattering paths B–O–B' that were therefore also included in the model.³⁷ Very good fit quality and relatively low bond length disorder verified that the B' atom was predominantly Sc(Ta) when B was Ta (Sc) and the Ta–O–Sc linkages are indeed quasicollinear.

Numerical results for the Ta *L*₃ and Sc *K*-edge analyses in the r range beyond the 1NN shell are summarized in Tables IV and VI, respectively. The lengths of the Ta–O–Sc linkage as measured by EXAFS from both ends, Ta and Sc, were

found equal, within the error bars, to each other. The lengths of these linkages are very close to the independently measured pseudocubic lattice constants a at all concentration x from 0 to 0.2 (Tables IV and VI). We believe the small discrepancy between the so obtained Ta–O–Sc distances and the lattice parameters is the indication that some fraction of Ta–O–Ta, Sc–O–Sc, Ta–O–Ti, and Sc–O–Ti linkages may be present in the samples but was not included in the multiple-scattering analysis of the distant r range using B-site ordering model. Because the discrepancy is very small ($a-r_3=0.03-0.04$ Å) compared to the Sc–O and Ta–O bond length mismatch, the fraction of such linkages must be small too.

In their study of order–disorder in perovskite ferroelectrics, Stenger and Burggraaf calculate that for completely ordered PST the areas of the (111) superlattice line, as measured by XRD, and the fundamental (200) peak, are in the ratio of 1.33 to 1.⁸ It should be noted that these authors state that for disordered PST starting material "...a slightly increased background can be observed around 2θ values where the superstructure lines might be expected. This may point to some kind of short-range ordering."⁸ Our XRD results obtained in the pure PST also showed a weak enhancement in the diffraction intensity in the vicinity where one would expect a sharp (111) superlattice peak in an ordered sample. The degree of ordering may differ between differently prepared PST samples because varying degrees of B site order can be produced in PST by varying the heat treatment.

Subsequent to the study of Stenger and Burggraaf, Baba-Kishi and Barber studied PST by transmission electron microscopy (TEM).³⁸ These authors reported ordered domains in PST where the domain size varies with heat treatment. Randall and Bhalla have carried out further TEM studies of PST and have reviewed this field for many related Pb(B'B'')O₃ perovskites.³⁹ Randall and Bhalla classify these compounds into three categories as follows: (a) materials for which no B site cation order is detected; (b) materials which exhibit B site cation order, but have a short coherent length of long range order; and (c) materials with B site order and a long coherent length of long range order. A short coherent length is defined to be in the range of approximately 20 to 800 Å in diameter, whereas a long coherent length is much larger than 1000 Å. Randall and Bhalla place PST into a category of material that always forms at least short coherent lengths of B site long range order, and can form long coherent lengths of B site long range order. These authors also report their own TEM result in which nanoscale B site ordered domains are observed in PST.

Based on all the above evidence, one would expect that XAFS studies, which sample the local environment on the atomic size scale, would yield results on (PST)_{1-x}(PT)_x consistent with B site order, even for samples that are largely disordered as measured by XRD. This conclusion is consistent with our XAFS results for the Sc–O and Ta–O distances in pure PST and with the multiple-scattering analysis of Ta and Sc local atomic environment in the extended r -range that includes the single scattering path to the 2NN Pb as well as single- and collinear multiple-scattering paths between the central Ta(Sc) atom, 1NN O, and the 3NN Sc(Ta) in the same direction.

Another main result of the multiple edge XAFS studies of the $(\text{PST})_{1-x}(\text{PT})_x$ system is an elucidation of the difference between the local structure of TiO_6 , TaO_6 , and ScO_6 octahedra at different x . As described above, the local structures of these octahedra, obtained by our combined EXAFS and XANES analyses, are different: Ti is off center, and Ta and Sc are on the center of the BO_6 octahedra. The present observation that the local structure of a TiO_6 octahedron is very different from the local structures of TaO_6 and ScO_6 octahedra in $(\text{PST})_{1-x}(\text{PT})_x$ mixture has a familiar ring relative to the recently observed effect in a rhombohedral ferroelectric $(\text{PbHfO}_3)_{0.9}(\text{PbTiO}_3)_{0.1}$.⁴⁰ In that system, analyzed by XAFS, it was found that the structure of the TiO_6 octahedron is very different from the structure of the HfO_6 octahedron.

The possibility to observe, with EXAFS, the short and long B–O (where B=Ti,Sc,Ta) bond lengths exists, theoretically, if their split δ is sufficiently large for the beat in k space of EXAFS data occurring at $\pi/(2\delta)$ to be detected. That means the beat should occur below the upper boundary of the data k range. Had the beat occurred at the highest available k value of 13 \AA^{-1} for Ta EXAFS data (Table III), or 10 \AA^{-1} for Sc EXAFS data (Table V), the corresponding values of δ_{Ta} and δ_{Sc} would have been equal to 0.12 \AA or 0.16 \AA , respectively. That means, within the present EXAFS data quality we can place the upper bounds on the Ta and Sc atom displacements $d = \sqrt{3}\delta/2$ at $d_{\text{Ta}} = 0.10 \text{ \AA}$ and $d_{\text{Sc}} = 0.14 \text{ \AA}$. By examining the Sc K -edge XANES data (Fig. 2), we conclude that d_{Sc} should not exceed the reference (dynamic) Ti atom displacement $d_{\text{Ti}} = 0.103 \text{ \AA}$ in EuTiO_3 at room temperature.¹⁸ Therefore, we can further lower the upper limit for d_{Sc} down to ca. 0.10 \AA . Without accurate temperature dependent study of EXAFS and XANES data it is impossible to distinguish, within the present data quality, the centrosymmetric from the noncentrosymmetric model of the Ta and Sc atoms environments. However, we can claim that the Ta or Sc atom displacements from the inversion symmetry center relative to the cubic cell as described in Kittel⁹ do not exceed ca. 0.10 \AA . On another hand, the Ti K -edge XAFS data allow us to determine the magnitude (by both EXAFS and XANES) and direction (by EXAFS) of Ti atom displacement from the inversion symmetry center at $x = 0.05$ unambiguously. In this case the displacement [$d = 0.22(2) \text{ \AA}$, Table I] is very large and the concomitant split in Ti–O distances [$d = 0.26(4) \text{ \AA}$] is detectable by EXAFS analysis.

CONCLUSIONS

We propose the following scenario of coordination-dependent structural transformations in $(\text{PST})_{1-x}(\text{PT})_x$ based on the combination of XANES and EXAFS results obtained

for Ti and Sc K edges and Ta L_3 edge. At low Ti concentrations, Ta is squeezed by its six oxygen neighbors into a smaller octahedral cage than the neighboring ScO_6 octahedra, due to their ionic radii difference. In both cases, these atoms are, approximately, on center in their octahedra. Lattice compression caused by the increase in the PbTiO_3 concentration is responsible for the gradual decrease in Ta–O distances.

However, because the average lattice parameter is larger than that for PbTiO_3 , small amounts of Ti have to be placed in larger octahedral units than their native PbTiO_3 cells. In these larger cells, the energetics favor (111) displacements, rather than (001) displacements off center. There will then be coexisting regions in the crystal; larger regions of PbTiO_3 take on a (001) distortion, and smaller regions take on a (111) distortion. Experimentally, we obtained that with increasing Ti concentration the average displacement direction gradually rotates from (111) to (001). The latter result provides direct experimental information for testing ab initio theories. Among the most adequate theories is the Maaskant-Bersuker model that explains this average rotation by the increase of the weighting factor of the 001-distorted PbTiO_3 unit cells in the sample as the concentration of PbTiO_3 increases. This model is consistent with our data. However, our results do not exclude the possibility, as obtained recently for other similar relaxor perovskites, of local gradual rotation between trigonal (rhombohedral) and tetragonal models of displacement of Ti atoms. These theories, yet to be developed for the $(\text{PST})_{1-x}(\text{PT})_x$ system, may also be directly compared with our data.

Another significant result is that all our $(\text{PST})_{1-x}(\text{PT})_x$ samples have a local ordering of the B sites with alternate occupation of Ta and Sc atoms extending over a nanoscale correlation length of at least several lattice constants.

ACKNOWLEDGMENTS

We are indebted to Professor L. E. Cross and Professor A. S. Bhalla for fruitful discussions. We appreciate the assistance of Jack Gromek with the x-ray diffraction studies and Poorani Pathmanabaiyer with the collection of Ta L -edge data. A.I.F. acknowledges support by the U.S. Department of Energy Grant No. DE-FG02-03ER15477, and E.A.S. and D.L.B. acknowledge support by the U.S. Department of Energy Grant No. DE-FG03-97ER45628. The NSLS is supported by the Divisions of Materials and Chemical Sciences of DOE. PNC-CAT is supported by the U.S. Department of Energy under Grant No. DE-FG03-97ER45628, the University of Washington, Pacific Northwest National Laboratory, and the Natural Sciences and Engineering Research Council of Canada. Use of the Advanced Photon Source was supported by DOE Contract No. W-31-109-Eng-38.

- *Author to whom correspondence should be addressed. Electronic address: frenkel@bnl.gov
- †Deceased.
- ¹L. E. Cross, *Ferroelectrics* **76**, 241 (1987).
 - ²M. E. Lines and A. M. Glass, *Principles and Applications of Ferroelectrics and Related Materials* (Clarendon, Oxford, 1977), p. 241.
 - ³G. A. Smolenskii and A. I. Agranovskaya, *Sov. Phys. Solid State* **1**, 1429 (1959); G. A. Smolenskii, *J. Phys. Soc. Jpn.* **28**, Suppl 26 (1970).
 - ⁴S. B. Vakhrushev, B. Kvyatkovsky, A. Nabereznov, N. Okuna, and B. Toperverg, *Ferroelectrics* **90**, 173 (1989).
 - ⁵R. Blinc, J. Dolinsek, A. Gregorovic, B. Zalar, C. Filipic, Z. Kutnjak, A. Levstik, and R. Pirc, *Phys. Rev. Lett.* **83**, 424 (1999); A. A. Bokov and Z. G. Ye, *Phys. Rev. B* **65**, 144112 (2002).
 - ⁶J. Tartaj, C. Moure, L. Lascano, and P. Duran, *Mater. Res. Bull.* **36**, 2301 (2001).
 - ⁷N. Sicon, B. Ravel, Y. Yacoby, E. A. Stern, F. Dogan, and J. J. Rehr, *Phys. Rev. B* **50**, 13168 (1994).
 - ⁸C. G. F. Stenger and A. J. Burggraaf, *Phys. Status Solidi A* **61**, 275 (1980).
 - ⁹C. Kittel, *Introduction to Solid State Physics*, 7th ed. (Wiley, New York, 1996).
 - ¹⁰R. Sommer, N. K. Yushin, and J. J. Van den Klink, *Phys. Rev. B* **48**, 13230 (1993).
 - ¹¹W. Dmowski, M. K. Akbas, P. K. Davies, and T. Egami, *J. Phys. Chem. Solids* **61**, 229 (2000).
 - ¹²J. R. Giniewicz, Ph.D. thesis, The Pennsylvania State University, 1991.
 - ¹³T. R. Shrout and A. Halliyal, *Am. Ceram. Soc. Bull.* **66**, 704 (1987).
 - ¹⁴Y. Yamashita, *Jpn. J. Appl. Phys., Part 1* **32**, 5036 (1993).
 - ¹⁵PbTiO₃ and EuTiO₃ XAFS data, measured in transmission, were made available courtesy of Bruce Ravel.
 - ¹⁶D. M. Pease, M. Daniel, J. I. Budnick, T. Rhodes, M. Hammes, D. M. Potrepka, K. Sills, C. Nelson, S. M. Heald, D. L. Brews, A. I. Frenkel, I. Gregorieva, and A. Antonov, *Rev. Sci. Instrum.* **71**, 3267 (2000).
 - ¹⁷L. A. Grunes, *Phys. Rev. B* **27**, 2111 (1983).
 - ¹⁸B. Ravel, Ph.D. thesis, University of Washington, 1995; B. Ravel, E. A. Stern, R. I. Vedrinskii, and V. Kraizman, *Ferroelectrics* **206**, 407 (1998).
 - ¹⁹V. Kraizman, A. Novakovich, R. Vedrinski, and V. Timoshevskii, *Physica B* **208&209**, 35 (1995).
 - ²⁰R. J. Nelmes, R. O. Plitz, W. F. Kuhs, Z. Tun, and R. Restori, *Ferroelectrics* **108**, 165 (1990).
 - ²¹M. Newville, P. Livins, Y. Yacoby, J. J. Rehr, and E. A. Stern, *Phys. Rev. B* **47**, 14126 (1993).
 - ²²S. I. Zabinsky, J. J. Rehr, A. Ankudinov, R. C. Albers, and M. J. Eller, *Phys. Rev. B* **52**, 2995 (1995).
 - ²³For our estimate of the lattice constants, we assumed that the 2θ value of the (200) peak is equal to that 2θ value corresponding to the most intense portion of the diffraction profile (Fig. 1). We then obtained pseudocubic lattice constants for $x=0, 0.05, 0.1,$ and 0.2 that agree with those obtained by Giniewicz on similar samples (Ref. 12), within the size of the points she uses to plot her results. Because of the varying width and asymmetry of these XRD peaks, we choose not to attempt a lattice constant determination by means more involved than this simple method.
 - ²⁴S. Teslic, T. Egami, and D. Viehland, *J. Phys. Chem. Solids* **57**, 1537 (1996).
 - ²⁵W. J. A. Maaskant and I. B. Bersuker, *J. Phys.: Condens. Matter* **3**, 37 (1991).
 - ²⁶B. Noheda, J. A. Gonzalo, A. C. Caballero, C. Moure, D. E. Cox, and G. Shirane, *Appl. Phys. Lett.* **74**, 2059 (1999); B. Noheda, J. A. Gonzalo, L. E. Cross, R. Guo, S.-E. Park, D. E. Cox, and G. Shirane, *Phys. Rev. B* **61**, 8687 (2000); B. Noheda, D. E. Cox, G. Shirane, R. Guo, B. Jonew, and L. E. Cross, *Phys. Rev. B* **63**, 014103 (2001); Z.-G. Ye, B. Noheda, M. Dong, D. Cox, and G. Shirane, *Phys. Rev. B* **64**, 184114 (2001).
 - ²⁷Z. Wu and H. Krakauer, *Phys. Rev. B* **68**, 014112 (2003).
 - ²⁸L. Bellaiche, A. Garcia, and D. Vanderbilt, *Phys. Rev. Lett.* **84**, 5427 (2000).
 - ²⁹H. Fu and R. E. Cohen, *Nature (London)* **403**, 281 (2000).
 - ³⁰V. Yu. Topolov, *Phys. Rev. B* **65**, 094207 (2002).
 - ³¹D. Vanderbilt and M. H. Cohen, *Phys. Rev. B* **63**, 094108 (2001).
 - ³²I. A. Sergienko, Yu. M. Gufan, and S. Urazhdin, *Phys. Rev. B* **65**, 144104 (2002).
 - ³³J. B. Newkirk, *J. Met.* **8**, 1214 (1956); A. Onodera, Y. Tsunoda, N. Kutinoma, O. A. Pringle, R. M. Nicklow, and R. M. Moon, *Phys. Rev. B* **50**, 3532 (1994); V. L. Moruzzi, P. M. Marcus, and J. Kubler, *ibid.* **39**, 6957 (1989).
 - ³⁴R. D. Shannon, *Acta Crystallogr., Sect. A: Cryst. Phys., Diffr., Theor. Gen. Crystallogr.* **A32**, 751 (1976).
 - ³⁵A. I. Frenkel, D. M. Fanning, D. L. Adler, I. K. Robinson, and J. O. Cross, in *First-Principles Calculations for Ferroelectrics*, edited by R. E. Cohen (AIP, Woodbury, NY, 1998), p. 96.
 - ³⁶M. Furuya, T. Mori, and A. Ochi, *J. Appl. Phys.* **75**, 4144 (1994).
 - ³⁷A. I. Frenkel, F. M. Wang, S. Kelly, R. Ingalls, D. Haskel, E. A. Stern, and Y. Yacoby, *Phys. Rev. B* **56**, 10869 (1997).
 - ³⁸K. Z. Baba-Kishi and D. J. Barber, *J. Appl. Crystallogr.* **23**, 43 (1990).
 - ³⁹C. A. Randall and A. S. Bhalla, *Jpn. J. Appl. Phys., Part 1* **29**, 327 (1990).
 - ⁴⁰N. Sicon, E. A. Stern, and Y. Yacoby, *J. Phys. Chem. Solids* **61**, 243 (2000).